JOURNAL OF CHEMICAL & ENGINEERING DATA

ARTICLE

pubs.acs.org/jced

Sorption of Copper(II) and Nickel(II) Ions from Aqueous Solutions Using Calcium Oxide Activated Date (*Phoenix dactylifera*) Stone Carbon: Equilibrium, Kinetic, and Thermodynamic Studies

Mohammed Danish,[*,†,‡] Rokiah Hashim,[†] M. N. Mohamad Ibrahim,[‡] Mohd Rafatullah,[†] Othman Sulaiman,[†] Tanweer Ahmad,[†] M. Shamsuzzoha,[§] and Anees Ahmad[∥]

[†]School of Industrial Technology, and [‡]School of Chemical Sciences, Universiti Sains Malaysia, 11800 Penang, Malaysia

[§]Department of Chemical Engineering, K.F.U.P.M., Dammam 31261, Saudi Arabia (KSA)

[∥]Analytical and Environmental Divison, Department of Chemistry, Aligarh Muslim University Aligarh-202002, India

Supporting Information

ABSTRACT: In this study, calcium oxide activated *Phoenix dactylifera* (commonly known as Date palm) stone carbon (ADS) was prepared, characterized, and used as a unconventional adsorbent for the removal of Cu(II) and Ni(II) ions from aqueous solutions in a batch process. The obtained activated carbon was characterized for pore size distribution and total surface area using BET isotherm, surface morphology using scanning electron microscopy, and surface functional groups using Fourier transform infrared spectroscopy, and the amorphous nature of the ADS was confirmed by X-ray diffraction studies. The kinetic data obtained at different temperatures were analyzed by applying pseudofirst-order, pseudosecond-order, and Weber-Morris diffusion models, as well as the Elovich equation. The applicability of Langmuir, Freundlich, and Dubinin−Radushkevich (D-R) adsorption isotherms was evaluated to better understand the adsorption process. The results of this study revealed that ADS has a honeycomb like surface morphology with large mesoporous surface area (645.5 $m^2 \cdot g^{-1}$) for adsorption and removal of copper and nickel was followed the pseudosecond-order kinetics and Langmuir model of isotherms. Thermodynamic studies revealed that the heat of adsorption of Cu(II) and Ni(II) ions was −4.99 $kJ \cdot mol^{-1}$ and −10.78 $kJ \cdot mol^{-1}$, respectively, which suggested that the adsorption was exothermic in nature.

INTRODUCTION

Pristine sources of water are now becoming polluted due to an increase in unsafe industrial practices around the world. The discharge of toxic heavy metal ions into water is a serious problem that may affect the quality of groundwater. In particular, pollution by metal ions has become a paramount issue in many countries because the concentration of metal ions in potable water and wastewater often exceeds admissible standards. The discharge of wastewater from industrial processes is a prime source of heavy metal pollution. If these effluents are discharged without treatment, they can have an adverse effect on the environment and human health. Owing to their toxic effects on wildlife and human beings, heavy metal ions such as copper, chromium, cadmium, lead, zinc, nickel, etc. must be removed from industrial wastewater.

Copper is introduced into groundwater and surface water through the production of pulp and paper board, and the preservation of wood and leather, as well as petroleum refining and copper smelting industries. For instance, in the wastewater of a typical copper wire mill, the average concentration of Cu ions is approximately 800 $mg \cdot L^{-1}$; however, water containing more than 1.0 $mg \cdot L^{-1}$ of Cu(II) is toxic to humans and animals.[1] Large doses of copper lead to severe mucosal irritation and corrosion, widespread capillary damage, hepatic and renal damage, and central nervous system irritation, which can lead to depression, severe gastrointestinal irritation, and possible necrotic changes in the liver and kidneys.[2] The World Health Organization (WHO) and the United States Public Health Services (USPHS) limit the concentration of copper in all water sources to 1.5 and 1.0 ppm, respectively; however, the maximum recommended concentration of Cu(II) in drinking water is 1.0 ppm.[3]

Nickel is an essential trace element that is used in the electroplating industry and the production of several types of alloys. The toxic action associated with nickel includes vomiting, chest pain, and rapid respiration. Dermatitis is common among workers involved in the production of nickel jewelry, nickel plated watches, and nickel based detergents. Nickel is highly carcinogenic, and high levels of nickel induce the reduction of nitrogen and impair growth.[4] Thus, the WHO limits the concentration of nickel in drinking water to 0.02 mg L^{-1}.[5]

Currently, many techniques such as chemical precipitation, evaporation, electroplating, phytoextraction, reverse osmosis, adsorption, and ion exchange are used for the treatment of heavy-metal-contaminated wastewater streams.[6−8] Thus, precipitation by lime, carbonates, sulphides or organosulphides has been applied to treat industrial wastewater. In addition, activated carbon has become a popular adsorbent for the removal of

Received: May 11, 2011
Accepted: August 11, 2011
Published: August 23, 2011

dx.doi.org/10.1021/je200460n | *J. Chem. Eng. Data* 2011, 56, 3607–3619

pollutants from wastewater.[9,10] However, the high cost of activated carbon limits its potential applications.[11] Therefore, a low cost and readily available adsorbent that can be used on a large scale must be developed.[12] Cheap and effective alternatives for the removal of heavy metals reduce operating costs and the prices of products, improve competitiveness, and benefit the environment. In previous studies, the adsorption capacities of a number of biomass based unconventional activated carbon (e.g., hazelnut husk, rubber wood sawdust, rice hulls, hazelnut shell, chestnut shell, grape seed, lotus stalk, palm shell, and date beads) have been determined.[13−20]

The aim of this study was to assess the ability of ADS to adsorb Cu(II) and Ni(II) ions from aqueous solutions. The effect of contact time, initial metal concentration, temperature, and adsorbent concentration on the removal of Cu(II) and Ni(II) ions from aqueous solution were evaluated. Moreover, the adsorption isotherms and probable mechanisms of adsorption were investigated. The kinetics and the order of the reaction at the surface of ADS, the thermodynamic parameters for the adsorption of Cu(II) and Ni(II), were also determined.

MATERIALS AND METHODS

Adsorbent Material: CaO Activated Date Stone. Dates (*Phoenix dactylifera*) were imported from Saudi Arabia. After removing the edible pulp, the stones were washed with water to remove the thin membrane adherent on the surface, as well as the remaining pulp material. After proper washing, the date stones were kept for drying in an oven at 378 K for 12 h. For chemical activation, the dried stones were impregnated in 200 mL of CaO solution (impregnation ratio, 2:1) for 24 h at room temperature (around 298.15 K). Upon completion, the date stone was separated from the solution and placed in a muffle furnace at 773 K for 2 h. The introduction of alkali or alkaline earth metals on the surface of the adsorbent provides basic sites that have a high affinity for adsorption. The basicity of a metal oxide decreases as the ratio of the electric charge to the radius of the metal ion increases. CaO has a low charge to radius ratio and can provide strong basic sites to the surface of the adsorbent.[20] Upon cooling, the material was ground with an electrical mixer, and ASTM (American Society for Testing Materials) sieves were used to limit the particle sizes of the material to approximately less than 250 μm (ASTM sieve no. 60) and bigger than 180 μm (ASTM sieve no. 80). The weights of the adsorbents were recorded to estimate weight loss during drying and carbonization (burning). The prepared adsorbent was carefully labeled and packed in airtight glass bottles.

Adsorbate Solution. A stock of 1000 mg·L^{-1} of Cu(II) and Ni(II) solutions were prepared by dissolving the corresponding chlorides ($CuCl_2 \cdot 2H_2O$ and $NiCl_2 \cdot 6H_2O$) in doubly distilled water. Prior to the adsorption experiments, the solutions were further diluted to the required concentrations. All the chemicals used in this study were of analytical grade and were obtained from Sigma-Aldrich and Fluka.

Characterization of ADS. The characterizations of the samples were carried out at their optimal working conditions. The activated carbon obtained after activation can be evaluated for burnoff percentage. Burn-off is defined as the weight difference between the precursor biomass and the activated carbon, divided by the weight of the precursor biomass, with both weights on a dry basis.[21] The following relationship was used for calculating the activation burnoff of date stone derived

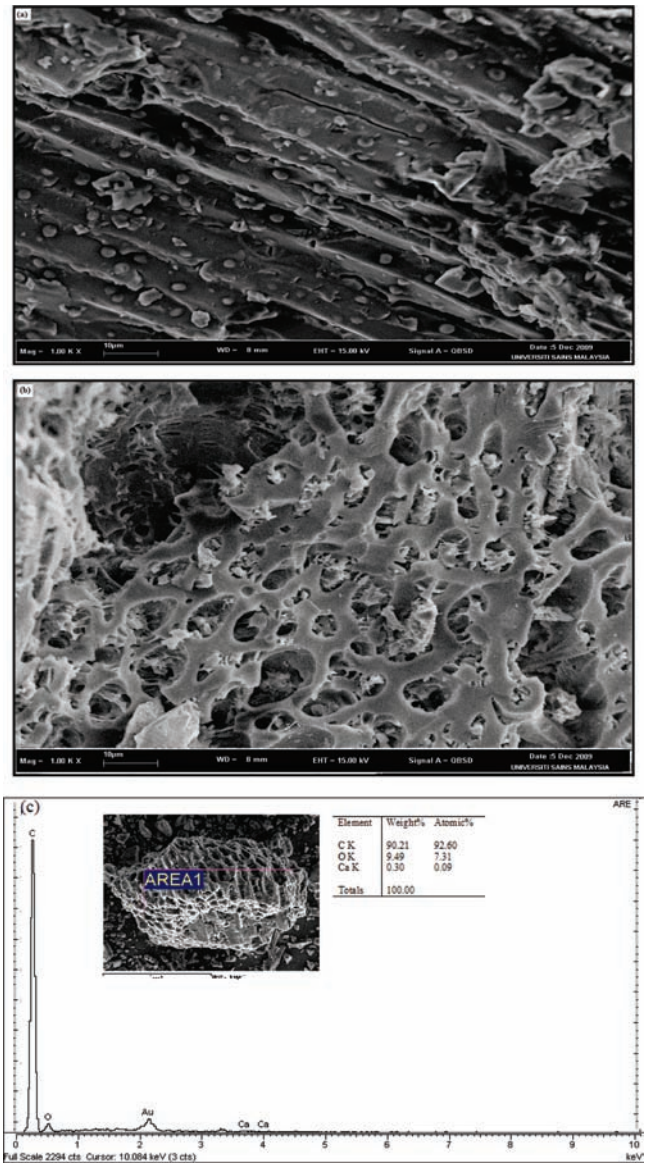

Figure 1. SEM micrograph of ADS (magnification, 1000): (a) before activation and (b) after activation and (c) EDX spectra of ADS.

activated carbon, ADS

$$\text{activation burn-off } \% = 100 - [\{\text{mass after activation(g)} / \text{precursor mass(g)}\} \times 100] \quad (1)$$

BET Surface Area Studies. Nitrogen adsorption isotherms were obtained at 77 K using a NOVA 2200e surface area and pore size analyzer. The specific surface area was determined by the BET isotherm equation, and the pore size distribution was calculated with the adsorption data based on original density functional theory. The samples were degassed for 12 h under vacuum at a temperature of 523 K prior to analysis to remove any impurities.

SEM and EDX Studies. A morphological and elemental composition study of the ADS was done with a Leo Supra 50 VP field emission scanning electron microscope (Carl-Ziess SMT, Oberkochen, Germany) equipped with an Oxford INCA 400 energy dispersive X-ray microanalysis system (Oxford

Instruments Analytical, Bucks, U.K.) that can give SEM and EDX with the same sample. The scanning electron micrograph (SEM) of the activated carbons at bar length equivalent to 10 μm, working voltage 15 kV with 1000× magnification are shown in Figure 1, panels a and b.

CHN Analysis. The ADS samples were analyzed for carbon, nitrogen, and hydrogen percentage content using CHN analyzer (model: Perkin-Elmer, Series 2, 2400). Purified helium was used as a carrier gas keeping flow rate 20 mL·min^{-1}. The combustion temperature of the furnace was kept at 1198 K; at this temperature, most of the ADS constituents were burned (if any substance that was not burned at this temperature cannot be detected by this instrument). The percentage error in the results is within ± 0.2 %.

FTIR Studies. The FTIR spectra of samples were recorded with an FTIR spectrophotometer Nicolet AVATAR 380 FT-IR model, using the potassium bromide (KBr) pellet method. Oven-dried solid samples of pure ADS and metal ions (nickel and copper) adsorbed ADS were thoroughly mixed with KBr in the ratio of 1:100 (weight ratio of sample to KBr). The solid mixture of activated carbon and KBr was ground to a very fine powder and then compressed at 15 000 psi (pound force per square inch) pressure to make a thin film disk for the spectra analysis. The spectra were recorded by 64 scan with 4 cm^{-1} resolution in the fingerprint spectral region of (4000 to 400) cm^{-1}

Powder XRD Analysis of ADS. The X-ray powder diffraction (XRD) measurements were performed by using Cu Kα radiation (40 kV, 30 mA, λ = 1.54 Å) with a step size of 0.05° glancing angle θ and with the holding time of 1 s at fixed θ. The 1 mm thick powder sample was placed on a plastic holder and the diffraction spectra were recorded at 298 K and treated by the Bruker DiffracPlus computer software. The XRD analysis was carried out on powder ADS samples to investigate the structural changes that occur during activation.

Batch Adsorption Studies. Adsorption studies were conducted at temperatures between (293 and 313) K and reaction time up to 180 min. In each experiment, 40 mg of ADS was added to 50 mL of a solution containing the desired concentration of metal ions in a stoppered conical flask, and the vials were agitated in a temperature-controlled shaker. After the predetermined time had elapsed, the reaction mixture was filtered, and the final concentration of metal ions in the filtrate was analyzed. The concentrations of Cu(II) and Ni(II) ions in aqueous solution were determined with an atomic absorption spectrometer (AAS; Analyst 100 Perkin-Elmer) equipped with an air−acetylene flame. The characteristic concentration of the AAS was found 0.088 ppm for Cu and 0.154 ppm for Ni. The adsorption experiments were also conducted to determine the optimal equilibrium time [(5 to 180) min], initial concentration of the adsorbate [(50 to 200) mg·L^{-1}], and temperatures [(293, 303, and 313) K]. All of the investigations were conducted in triplicate to avoid discrepancies in the experimental results. Moreover, control solutions were evaluated throughout the experiment to maintain quality control. The percentage of metal adsorption was computed according to the following equation:

$$\text{adsorption}\% = \{(C_i - C_e)/C_i\}100 \quad (2)$$

where C_i and C_e are the initial and equilibrium concentration of metal ions (mg·L^{-1}) in solution. The adsorption capacity was determined by calculating the mass balance equation for the adsorbent

$$q = (C_i - C_e)V/W \quad (3)$$

where q is the adsorption capacity (mg·g^{-1}), V is the volume of the metal ion solution (L), and W is the weight of the adsorbent (g).

Table 1. Physical Characteristics and Elemental Composition of ADS

parameters	units	value
BET surface area	$m^2 \cdot g^{-1}$	962.4899
total volume	$cm^3 \cdot g^{-1}$	0.477795
micropore surface area	$m^2 \cdot g^{-1}$	316.9676
mesopore surface area	$m^2 \cdot g^{-1}$	645.5223
mean pore diameter	Å	19.8566
burn-off	%	73.33
ash	%	1.3
carbon	%	89.45
nitrogen	%	0.14
hydrogen	%	2.13

RESULTS AND DISCUSSION

Characterization of ADS. The characteristics of ADS such as the burn off percentage, surface area, surface morphology, elemental constituents, crystalinity, surface functional groups bulk density, and ash content were analyzed and the results are indicated in Table 1. ADS had percentage burnoff 73.30 ± 0.20 %, which indicates that during pyrolysis most of the weight constituents of the date stones were unstable at a temperature around 773 K. The remaining part of the material contain 0.902 (in mass fraction) of carbon (calculated by EDX analysis), which are expected to have graphitic structure.

Figure 1, panels a and b, shows the SEM micrographs of ADS before and after activation. It can be vividly seen from the micrographs that after activation with CaO the surface changes from sheet type layered structure to honeycomb like morphology. This microhole morphology contains mostly carbon atoms in the network chain. This hypothesis, supported by EDX and CHN study of ADS and the EDX plot as shown in Figure 1c, revealed that the elemental composition of the activated carbon-(ADS) possessed a high percentage of carbon (w = 0.9021) and second prominent atom in the network is oxygen (w = 0.949). Around 0.0030 mass fraction of calcium atom was also reported in the plot, and the amount is negligible and may remain as an impurity with the carbon surface. Based on the morphology and elemental constituents of the material, ADS appeared to be a suitable adsorbent.

Physisorption technique was used for the textural characterization of the prepared activated carbon, ADS. The surface area and the pore size distribution of the ADS were determined and are reported in table 1. The textural characterization however has been reported in Table 2. The surface area and pore size distribution were determined by the volumetric adsorption of N_2 by the ADS at 77 K and have been reported in Figure 2, panels a and b. The BET experiments provide data for the determination of the monolayer adsorbed amount, apparent specific surface area, pore volume, and pore size distribution by using density functional theory (DFT). The micropore and mesopore can be defined by the hysteresis during adsorption at relatively high relative pressure (P/P_0). The mesopore surface area was

Table 2. BJH Adsorption Pore Distribution Report of ADS

pore diameter range (Å)	average diameter (Å)	incremental pore vol. ($cm^3 \cdot g^{-1}$)	cumulative pore vol. ($cm^3 \cdot g^{-1}$)	incremental pore area ($m^2 \cdot g^{-1}$)	cumulative pore area ($m^2 \cdot g^{-1}$)
1710.0−1381.3	1510.4	0.000345	0.000345	0.009	0.009
1381.3−1069.7	1185.6	0.000492	0.000837	0.017	0.026
1069.7−838.8	926	0.000438	0.001275	0.019	0.045
838.8−675.1	738.9	0.000454	0.001728	0.025	0.069
675.1−542.7	594.1	0.000323	0.002052	0.022	0.091
542.7−422.9	467.5	0.000523	0.002575	0.045	0.136
422.9−333.6	367.3	0.000423	0.002998	0.046	0.182
333.6−268.3	293.5	0.000634	0.003632	0.086	0.268
268.3−213.7	234.5	0.000669	0.004301	0.114	0.382
213.7−164.2	182	0.00076	0.005061	0.167	0.549
164.2−129.4	142.3	0.001079	0.00614	0.303	0.852
129.4−103.8	113.5	0.001268	0.007407	0.447	1.299
103.8−80.3	88.7	0.00212	0.009528	0.956	2.255
80.3−59.6	66.4	0.003957	0.013485	2.383	4.639
59.6−45.8	50.6	0.006873	0.020357	5.435	10.074
45.8−36.7	40	0.010552	0.030909	10.542	20.616
36.7−30.5	32.9	0.017012	0.047921	20.71	41.326
30.5−24.7	26.8	0.042747	0.090668	63.813	105.139
24.7−19.3	21.1	0.110998	0.201666	210.016	315.154

calculated 645.523 $m^2 \cdot g^{-1}$ which indicates that the ADS can be used as potential adsorbent.

A quantitative analysis of carbon, nitrogen, and hydrogen through CHN analysis report enable us to verify the EDX results. It was observed that carbon percentage (w = 0.8945 in mass fraction) was in close agreement with EDX, whereas hydrogen (w = 0.0213 in mass fraction) cannot be detected by EDX. A small percentage of nitrogen (w = 0.0014 in mass fraction) was also reported in CHN results that was absent in the EDX.

FTIR spectra were recorded before and after the adsorption of Cu(II) and Ni(II) separately as presented in Figure 3. The FTIR spectrum of the ADS pre- and postadsorption condition provide information of the chemical structure and surface functional groups changes on adsorption of nickel and copper. The spectra of pure ADS has distinguished peaks at 2923.29 cm^{-1} (due to asymmetric C−H stretching of methylene groups in aliphatic compounds or fragments) and 2855.79 cm^{-1} (symmetric C−H vibration of methylene groups in aliphatic compounds or fragments), but after adsorption of Ni(II) and Cu(II), these peaks were almost extinct. ADS has no peak at 2359.50 cm^{-1} (characteristic to multiple bonding between the atoms), but after Ni(II) and Cu(II) adsorption, a new peak generated at this frequency. These changes in the functional group frequency are probably due to the metal ion interaction with the electron rich sites in the ADS, which causes the shift of peak from 2923.04 cm^{-1} and 2855.22 cm^{-1} to 2358.74 cm^{-1} (it is expected that methylene groups generate a multiple bond between the carbon atoms).[22] These two are the significant changes in the backbone chemical structure and functional groups of the ADS after metal ions (copper and nickel) adsorption, and the rest of the functional groups are unchanged during the adsorption.

Powder XRD patterns for the ADS were recorded and represented in Figure 4. The sample was found to be amorphous, although broad diffused peaks were observed at low angles. The diffraction peak of crystalline carbon was not observed. The

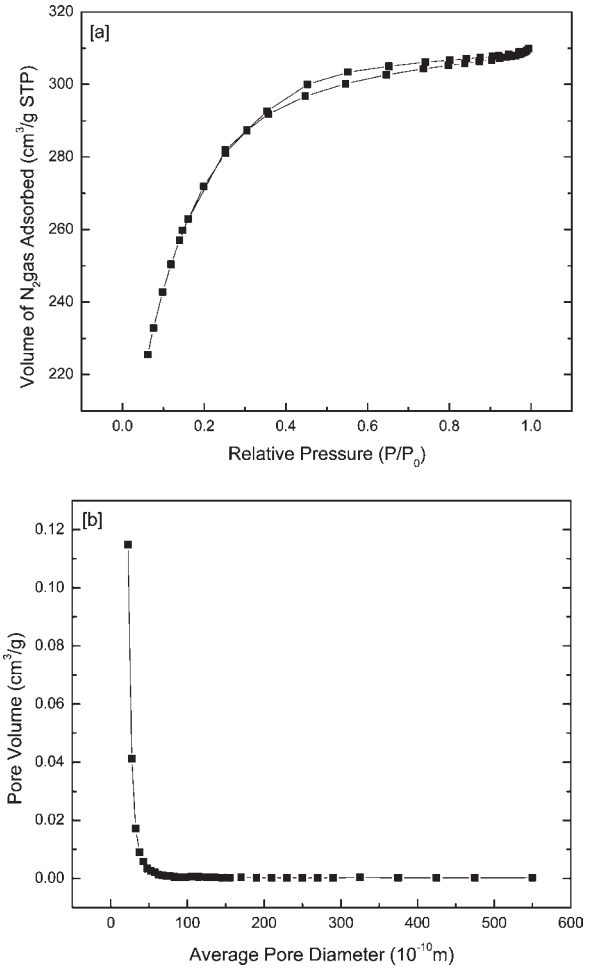

Figure 2. (a) Nitrogen adsorption isotherm of ADS at 77 K and (b) pore size distribution of ADS.

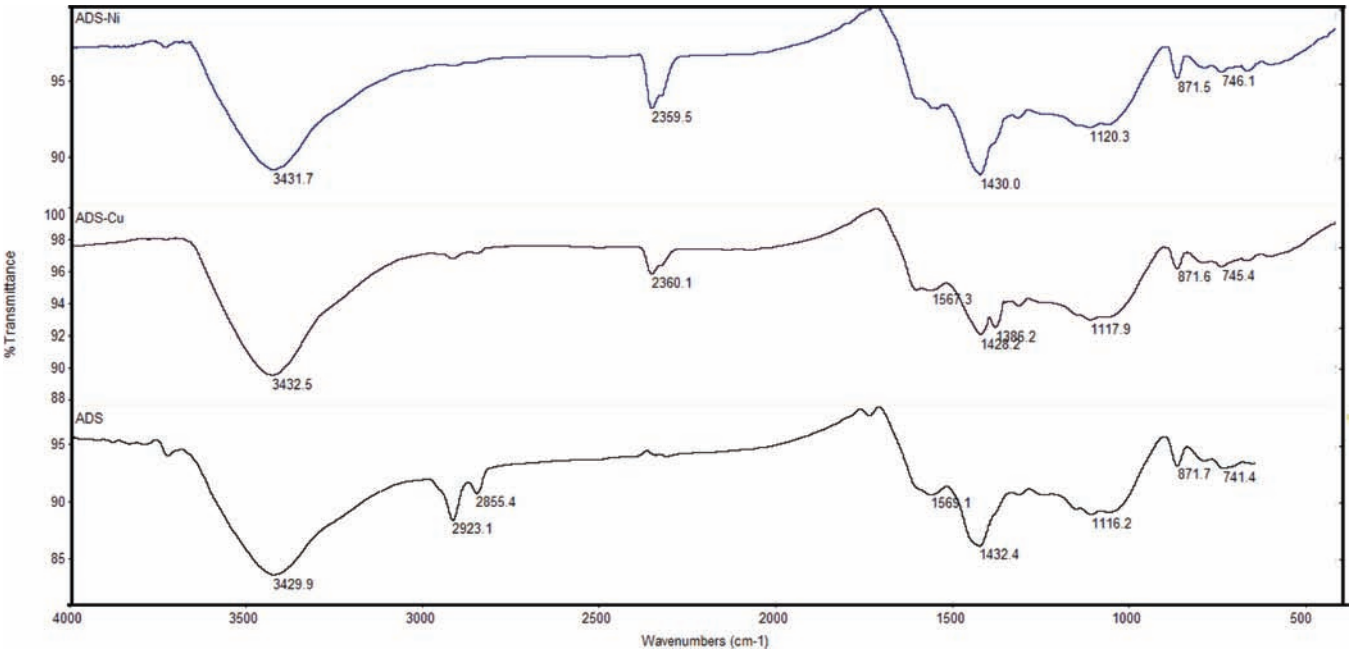

Figure 3. FTIR spectrum of pre- and postadsorption of copper and nickel ions on ADS.

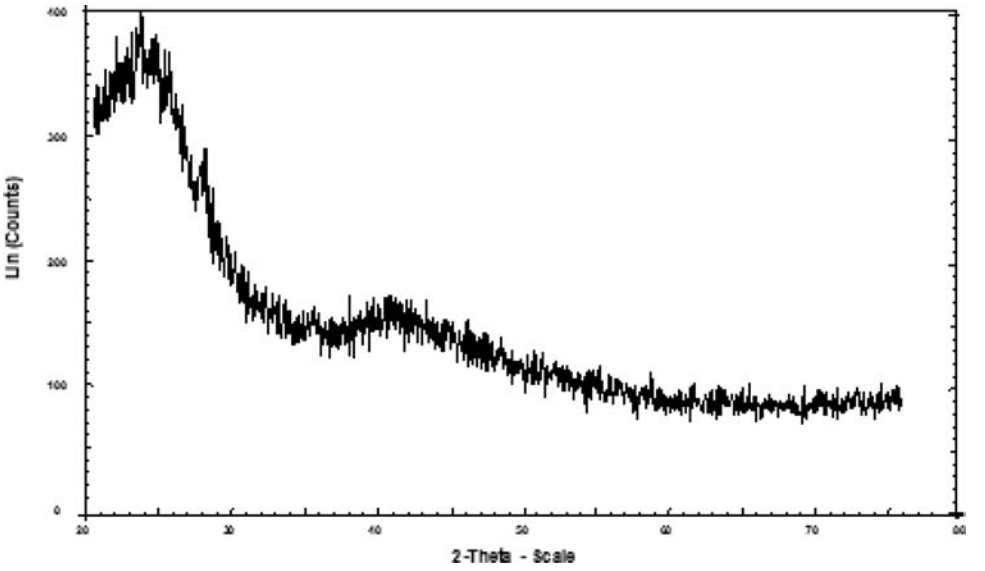

Figure 4. Characteristics powder XRD diffractogram of ADS carbon.

X-ray diffraction peak confirmed that ADS possesses a heterogeneous surface.

Effect of Contact Time and Initial Metal Concentration. In batch adsorption processes, the initial concentration of the adsorbate can act as a driving force to overcome mass transfer resistance between the solution and the solid phase. Therefore, the amount of metal ions adsorbed from solution was expected to increase as the initial concentration of metal ions increased. As shown in the plot of the equilibrium concentration of adsorbed Cu(II) and Ni(II) versus time at 293 K (Figure 5, panels a and b), the sorption capacity of ADS increased with an increase in the initial metal ion concentration. The amount of Cu(II) and Ni(II) adsorbed at equilibrium appeared to follow the same trend, and both ions increased as the initial metal ion concentration increased. The electronegativity of Cu(II) and Ni(II) ions are 1.90 and 1.80 (Pauling scale), respectively; thus, the greater electronegativity of Cu(II) may enhance the binding capacity of copper toward the negatively charged adsorbent surface, resulting in a slightly higher adsorption capacity for Cu(II) than Ni(II). The fact that the adsorbed equilibrium concentration increased with an increase in metal concentration indicates that ADS has immense potential as an adsorbent for the treatment of wastewater with high concentrations of metal ions. Moreover, the results shown in Figure 5, panels a and b, indicate that the rate of Cu(II) and Ni(II) adsorption is initially rapid and gradually decreases over time until equilibrium is attained because a large

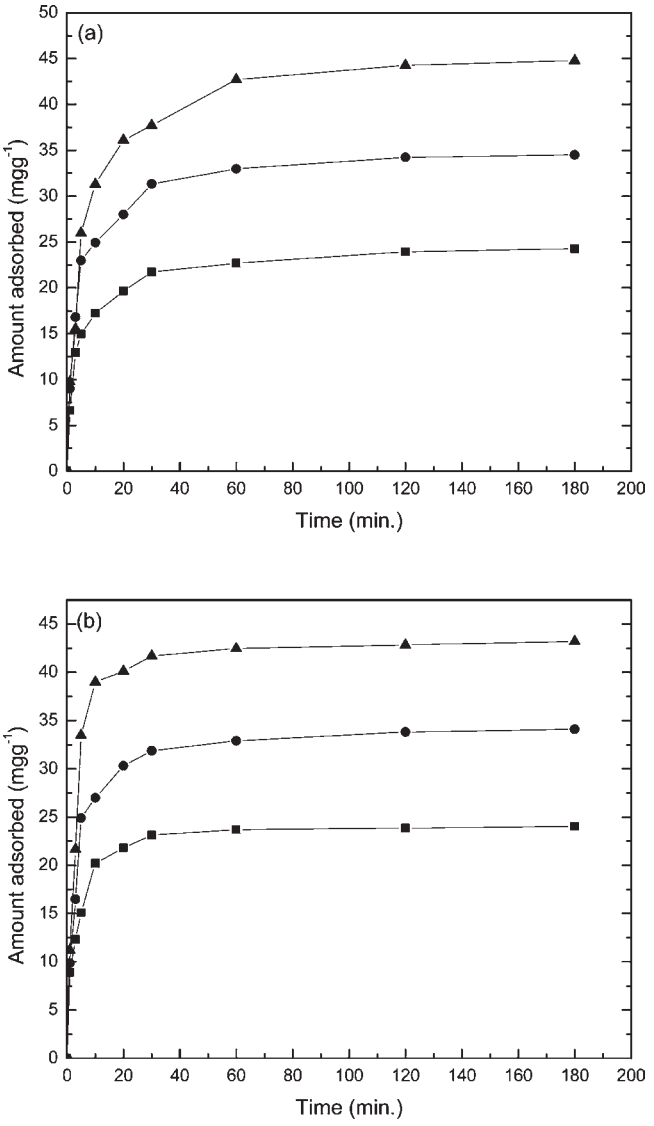

Figure 5. Effect of contact time and initial concentration on the adsorption of metal ions onto ADS: (a) Cu(II) and (b) Ni(II) [■, 50 mg·L^{-1}; ●, 100 mg·L^{-1}; ▲, 200 mg·L^{-1}; agitation speed = 150 rpm; temperature = 293 K; pH 6.0 for Cu(II) and pH 5.5 for Ni(II)].

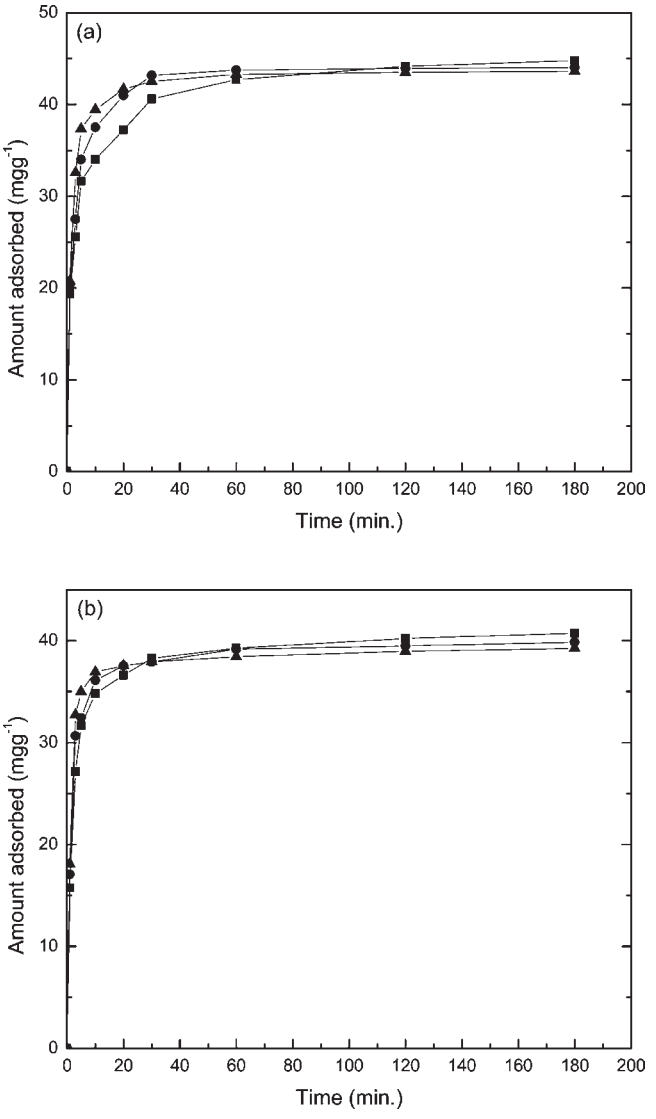

Figure 6. Effect of temperature on the adsorption of metal ions onto ADS: (a) Cu(II) and (b) Ni(II) [■, 293 K; ●, 303 K; ▲, 313 K; initial concentration = 100 mg·L^{-1}; agitation speed = 150 rpm; contact time = 180 min,; pH 6.0 for Cu(II) and pH 5.5 for Ni(II)].

number of surface sites are available for adsorption during the initial stages of the process. However, adsorption to the remaining vacant surface sites becomes difficult over time due to the repulsive forces between solute molecules on the solid phase. After shaking the solutions for 180 min, equilibrium was attained and the adsorption capacity of Cu (II) and Ni (II) ions did not change over time.

Effect of Temperature. Adsorption experiments were conducted to study the effect of temperature [(293 to 313) K] on the adsorption of Cu(II) and Ni(II) ions at an optimum pH of 6.0 and 5.5, respectively. The results suggested that the adsorption capacity of Cu(II) and Ni(II) increased from (19.39 to 44.79) mg·g^{-1} and (15.77 to 40.73) mg·g^{-1}, respectively, at temperature 293 K. As shown in Figure 6, panels a and b, the initial rate of adsorption of Cu(II) and Ni(II) ions was relatively high at greater temperatures. Moreover, in almost all of the experiments, total adsorption reached a constant value within 30 min. However, at equilibrium, the total adsorption was greater at lower temperatures, and the following trend for maximum adsorption was observed: 293 K > 303 K > 313 K. The observed trend in the total adsorption at equilibrium may be associated with the increase in kinetic energy of the ions at higher temperatures,[14] which causes a decrease in adsorption. The results revealed the exothermic nature of the adsorption process, which was verified by the determination of the change in the standard Gibbs free energy ($\Delta G°$), standard heat of adsorption ($\Delta H°$), and standard entropy ($\Delta S°$) of adsorption.

Adsorption Kinetics Studies. In this study, the kinetics of the adsorption of Cu(II) and Ni(II) ions were also evaluated. The kinetics of an adsorption process describes the rate of solute uptake and diffusion to the surface of the adsorbent, which controls the residence time of the adsorbate at the solid−liquid interface. The mechanism of adsorption depends on the physical and chemical characteristics of the adsorbents.[23] The results obtained from adsorption experiments were used to study the kinetics of Cu(II) and Ni(II) adsorption. The rate of the

Table 3. Pseudofirst-Order and Pseudosecond-Order Kinetic Models for the Adsorption of Cu(II) and Ni(II) onto ADS at Different Temperatures[a]

			pseudofirst order				pseudosecond order				
metal ions	temp. (K)	$q_{e,exp}$ (mg·g^{-1})	$q_{e,cal}$	k_1	SSE	R^2	$q_{e,cal}$	k_2	h	SSE	R^2
Cu(II)	293	2.84	1.208	$2.99\cdot10^{-2}$	0.293	0.885	2.882	$11.98\cdot10^{-2}$	0.995	0.329	0.999
	303	2.79	1.153	$4.84\cdot10^{-2}$	0.498	0.854	2.825	$24.62\cdot10^{-2}$	1.965	0.131	1.000
	313	2.76	1.393	$5.30\cdot10^{-2}$	0.536	0.888	2.786	$36.93\cdot10^{-2}$	2.865	0.053	1.000
Ni(II)	293	2.59	1.172	$2.99\cdot10^{-2}$	0.591	0.794	2.611	$19.77\cdot10^{-2}$	1.348	0.193	0.999
	303	2.53	1.560	$3.22\cdot10^{-2}$	0.536	0.740	2.545	$30.77\cdot10^{-2}$	1.992	0.111	1.000
	313	2.49	2.061	$3.22\cdot10^{-2}$	0.483	0.680	2.500	$43.01\cdot10^{-2}$	2.688	0.128	1.000

[a] $q_{e,cal}$ = (mg·g^{-1}), k_1 = (min^{-1}), k_2 = (gm·g^{-1}·min^{-1}), and h = (mg·g^{-1}·min^{-1}).

adsorption of Cu(II) and Ni(II) ions onto ADS was applied to the Lagergren pseudofirst-order model,[24] pseudosecond-order model,[25] Elovich equation,[26] and Weber−Morris diffusion model.[27] The conformity between experimental data and the predicted values of the model was expressed by the correlation coefficient (R^2). In addition, the fit of each model to the experimental data were evaluated by determining the corresponding sum of the squares of error (SSE), according to the following equation:

$$\mathrm{SSE} = \left(\frac{\Sigma(q_{exp} - q_{cal})^2}{N}\right)^{1/2} \quad (4)$$

where N is the number of data points, q_{exp} is experimentally calculated quantity, and q_{cal} is predicted quantity through model.

Pseudofirst-Order Kinetic Model. The Lagergren pseudofirst-order rate model is based on the capacity of the adsorbent and is generally expressed as follows:

$$\frac{dq}{dt} = k_1(q_e - q) \quad (5)$$

where q_e is the amount of solute adsorbed at equilibrium per unit weight of adsorbent (mg·g^{-1}), q is the amount of solute adsorbed at a given time (mg·g^{-1}), and k_1 is the adsorption constant. Equation 5 was integrated under the boundary conditions $t = 0$ to $t > 0$ ($q = 0$ to $q > 0$) and rearranged to obtain the following time dependent function:

$$\log(q_e - q) = \log(q_e) - (k_1/2.303)t \quad (6)$$

Equation 6 is the most popular form of the pseudofirst-order kinetic model. Values of k_1 at different temperatures were calculated from the plots of $\log(q_e - q)$ versus t for Cu(II) and Ni(II) ions. The value of k_1 in the pseudofirst-order kinetic model and the corresponding correlation coefficients (R^2) were calculated and are summarized in Table 3. The highest sums of square errors (SSE) were obtained for this set of data compared to pseudosecond-order kinetic set of data. The lowest correlation coefficient was 0.854 (SSE 0.498) for Cu(II) ions and 0.680 (SSE 0.483) for Ni(II) ions; thus, the model did not fit the experimental data.

Pseudosecond-Order Kinetic Model. The kinetic data were analyzed by applying the pseudosecond-order model to the experimental data. The pseudosecond-order kinetic model can be expressed as

$$\frac{dq}{dt} = k_2(q_e - q)^2 \quad (7)$$

After integrating eq 7 under the boundary conditions $t = 0$ to $t > 0$ and $q = 0$ to $q > 0$ and rearranging the equation, the following linearized form of the pseudosecond-order model was obtained

$$\frac{t}{q} = \left(\frac{1}{k_2 q_e^2}\right) + \left(\frac{1}{q_e}\right)t \quad (8)$$

$$h = k_2 q_e^2 \quad (9)$$

where h is the initial sorption rate (mg·g^{-1}·min^{-1}). A plot of t/q versus t should produce a straight line, and the values of q_e and k_2 can be determined from the slope and intercept of the plot (Figure 7, panels a and b). The values of k_2, q_e, and h are presented in Table 3, along with the corresponding correlation coefficients (R^2). It can be seen from the table that the initial sorption rate, h, increases at higher temperature in the case of both metal ions. The minimum correlation coefficients (R^2) for this model were 0.999 (SSE 0.193); however, most of the values reached 1.000 (SSE 0.053), and the sum of square error (SSE) values reached a minimum level which indicates that the model provided a perfect fit of the experimental data. Thus, the adsorption of Cu(II) and Ni(II) ions onto ADS follows the pseudosecond-order kinetic model.

Elovich Equation. The Elovich equation provides a kinetic model of the adsorption process and is expressed as

$$\frac{dq_t}{dt} = \alpha e^{-\beta q_t} \quad (10)$$

where q_t is the adsorption capacity at time t, α is the initial adsorption rate (mg·g^{-1}·min^{-1}), and β is the desorption constant (gm·g^{-1}). Equation 10 was integrated under the boundary conditions $q_t = 0$, to $q_t = q_t$ and $t = 0$ to $t = t$ and rearranged to obtain the following linear time dependent function:

$$q_t = \frac{1}{\beta}\ln(\alpha\beta) + \frac{1}{\beta}\ln t \quad (11)$$

A plot of q_t versus $\ln(t)$ should provide a straight line with a slope of $1/\beta$ and an intercept of $1/\beta \ln(\alpha\beta)$; thus, the value of α and β was obtained from the plot and is reported in Table 4. The correlation coefficients for this model were lower than those obtained with the pseudosecond-order kinetic model.

Weber−Morris Diffusion Model. The possibility of intraparticle diffusion was examined by applying the Weber−Morris diffusion model to the experimental data. According to the Weber−Morris diffusion model, the amount of adsorbed material is proportional to the square root of the contact time

$$q_t = k_d t^{1/2} + C \quad (12)$$

where k_d ($mg \cdot g^{-1} \cdot min^{-1/2}$) is the intraparticle diffusion constant and C is the intercept of the plot of eq 12 in units of $mg \cdot g^{-1}$. Equation 12 was applied to the adsorption data obtained at various contact times ranging from (5 to 180) min. McKay and Al-Duri[28] suggest that the shape of the first section of the Weber−Morris diffusion curve is attributable to boundary layer diffusion effects and the linear portion of the curve is a result of intra particle diffusion. The correlation coefficients of the Weber−Morris diffusion model were poor; thus, diffusion is not involved in the rate determining step of the adsorption process. The rate constant for intraparticle diffusion, k_d, and the correlation coefficient, R^2, were calculated from the respective plots and are provided in Table 4. The values of the correlation coefficients were not uniform or large enough to suggest that intraparticle diffusion was the rate determining step of the adsorption process.[29]

The rates of most chemical reactions increase markedly as the temperature of the reaction is increased, and the temperature dependence of the reaction appears in the rate constant of the rate law. Remarkably, the temperature dependence of almost all

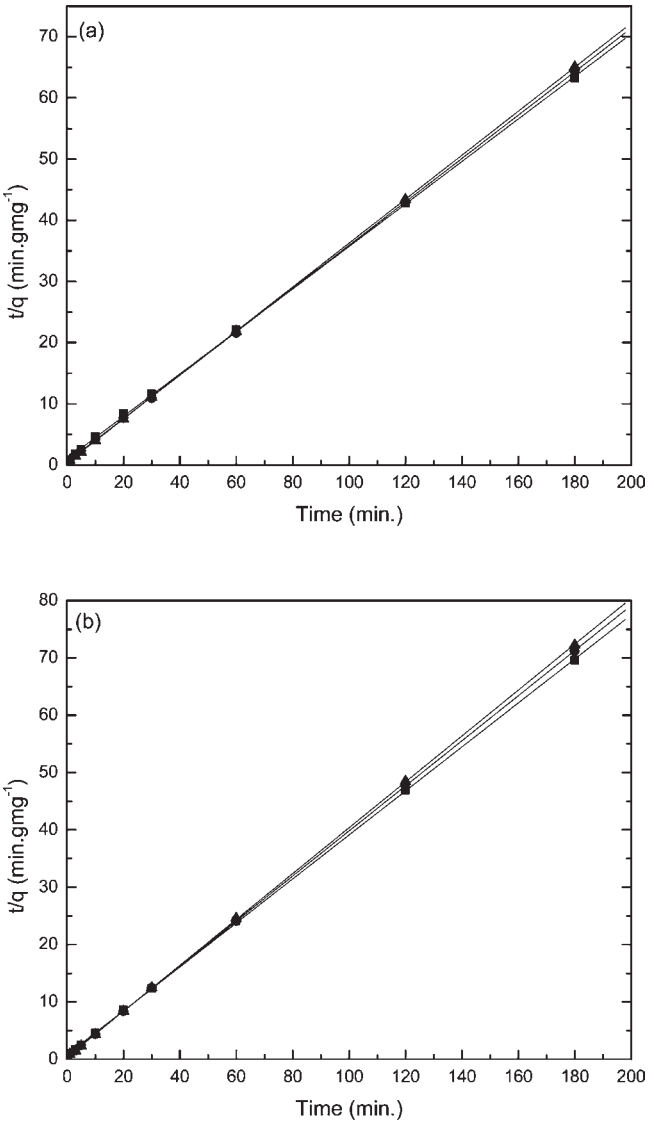

Figure 7. Pseudosecond-order kinetic plot of the adsorption of metal ions onto ADS at different temperatures: (a) Cu(II) and (b)Ni (II) [■, 293 K; ●, 303 K; ▲, 313 K; initial concentration = 100 $mg \cdot L^{-1}$; agitation speed = 150 rpm; contact time = 180 min; pH 6.0 for Cu(II) and pH 5.5 for Ni(II)].

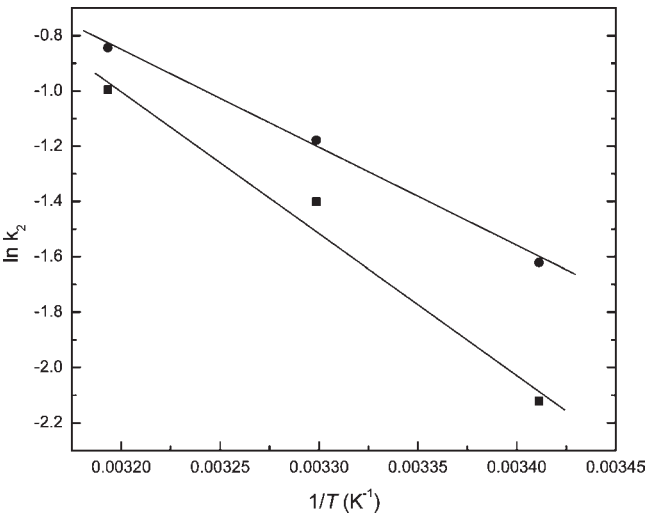

Figure 8. Arrhenius plots for the adsorption of Cu(II) (■) and Ni(II) (●) onto ADS.

Table 4. Thermodynamic Parameters and Arrhenius Constants for the Adsorption of Cu(II) and Ni(II) onto ADS[a]

		thermodynamic parameters						Arrhenius parameters			Elovich model		Weber−Morris model		
metal ions	temp. (K)	$\Delta G°$	$\Delta H°$	$\Delta S°$	SSE	R^2	E_a	A	SSE	R^2	β	α	k_d	C	R^2
Cu (II)	293	−4.965									3.185	24.57	0.276	1.164	0.901
	303	−5.029	−04.99	−0.012	0.021	0.952	43.07	$5.9 \cdot 10^6$	0.113	0.980	3.472	62.41	0.302	1.245	0.880
	313	−4.962									3.132	32.90	0.258	1.490	0.720
Ni (II)	293	−4.897									3.676	42.97	0.270	1.136	0.760
	303	−4.624	−10.78	−20.17	0.024	0.986	29.68	$3.9 \cdot 10^4$	0.033	0.996	4.310	17.04	0.239	1.308	0.670
	313	−4.497									5.076	90.87	0.210	1.462	0.557

[a] $\Delta G°$ = $kJ \cdot mol^{-1}$, $\Delta H°$ = $J \cdot mol^{-1}$, $\Delta S°$ = $kJ \cdot mol^{-1} \cdot K^{-1}$, E_a = $kJ \cdot mol^{-1}$, β = $gm \cdot g^{-1}$, α = $mg \cdot g^{-1} \cdot min^{-1}$, k_d = $mg \cdot g^{-1} \cdot min^{-1/2}$, C = $mg \cdot g^{-1}$.

dx.doi.org/10.1021/je200460n |J. Chem. Eng. Data 2011, 56, 3607–3619

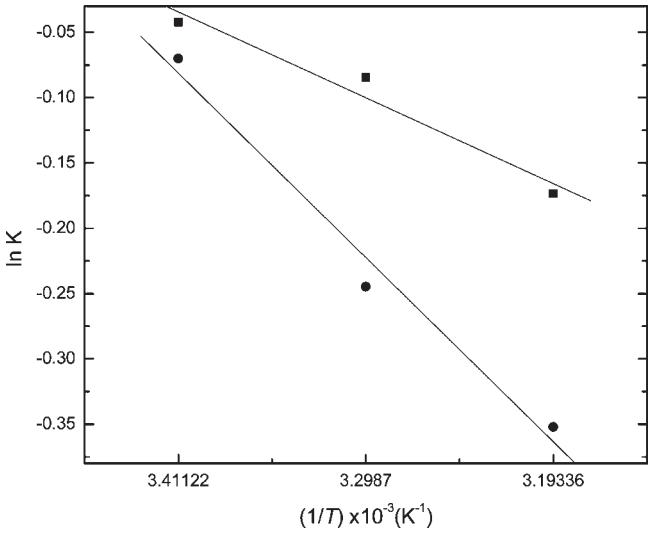

Figure 9. Plot of ln K versus $1/T$ for the adsorption of Cu(II) (■) and Ni(II) (●) onto ADS.

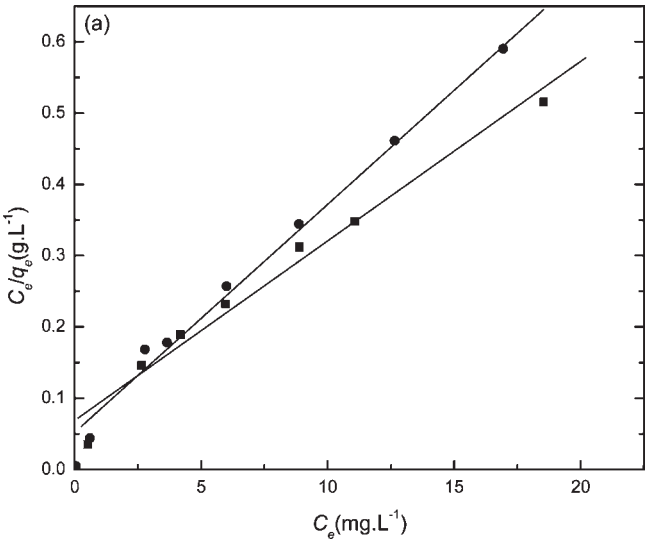

Figure 10. Langmuir isotherm plots of the adsorption of Cu(II) (■) and Ni(II) (●) onto ADS at 293 K.

reactions fit the Arrhenius equation.[30]

$$\ln k_2 = \ln(A) - \frac{E_a}{RT} \tag{13}$$

where k_2 is the rate constant of the pseudosecond-order kinetic model, E_a is the activation energy, and A is the Arrhenius frequency factor. To obtain the values of E_a and A from the kinetic data, a series of rate constants were measured at different temperatures and a plot of ln k_2 versus $1/T$ was generated, as shown in Figure 8. The slope of the plot of ln k_2 versus $1/T$ is the activation energy, E_a, and the intercept is the Arrhenius frequency factor, A. As shown in Table 4, activation energies of 43.07 kJ·mol^{-1} and 29.68 kJ·mol^{-1} were obtained for Cu(II) and Ni(II), respectively. Ho et al.[31] suggests that the activation energy of diffusion-controlled adsorption processes is less than 30 kJ·mol^{-1}. The activation energy of the adsorption of Cu(II) suggested that copper adsorption is not controlled by diffusion. Alternatively, the results indicated that the adsorption of nickel is affected by diffusion processes.

Thermodynamic Study of Adsorption. Thermodynamic parameters can provide information on the nature of the adsorption process; thus, the standard change in Gibbs free energy ($\Delta G°$), entropy ($\Delta S°$), and enthalpy ($\Delta H°$) were determined from the following equations:

$$\Delta G° = -RT \ln K \tag{14}$$

where R is the universal gas constant (8.314 J·mol^{-1}·K^{-1}), T is the absolute temperature (K), and the equilibrium constant K is the ratio of equilibrium concentration of adsorbate in liquid and in solid phase.

The standard enthalpy change ($\Delta H°$) from 293 to 313 K was obtained from the following equation:

$$\ln K = \frac{\Delta S°}{R} - \frac{\Delta H°}{RT} \tag{15}$$

As shown in Figure 9, a plot of ln K versus $1/T$ should provide a straight line, and the values of $\Delta H°$ and $\Delta S°$ were obtained from the slope and intercept of the plot, respectively. The standard free energy change ($\Delta G°$), enthalpy change ($\Delta H°$), and entropy change ($\Delta S°$) were obtained from eqs 14 and 15 and are shown in Table 4. The negative values of $\Delta H°$ and $\Delta G°$ indicates that the adsorption process was exothermic and spontaneous. The $\Delta H°$ values obtained for the adsorption of Cu(II) and Ni(II) ions were −4.99 kJ·mol^{-1} and −10.78 kJ·mol^{-1}, respectively, indicating that the adsorption process was based on chemical interactions. Moreover, the values of the activation energy of adsorption support these results. The negative values of $\Delta S°$ for the adsorption of Cu(II) and Ni(II) ions suggested that the randomness at the solid/liquid interface decreased during the adsorption process due to the complexation of negatively charged active sites and positively charged metal ions.

Adsorption Isotherm Models. The adsorption isotherms revealed the relationship between the concentration of the adsorbate and the extent of adsorption onto the surface of the adsorbent at a constant temperature. To quantify the adsorption capacity of ADS for the removal of Cu(II) and Ni(II) ions from aqueous solution, three isotherm models were applied to the experimental data, including the Langmuir, Freundlich, and Dubinin−Radushkevich (D-R) isotherm equations.

Langmuir Isotherm Model. The Langmuir model assumes that adsorption occurs at specific homogeneous sites on the adsorbent and can be successfully applied to monolayer adsorption processes. The data obtained from the equilibrium studies of the adsorption of Cu(II) and Ni(II) ions onto ADS may follow the Langmuir model, which can be expressed by the following equation:[32]

$$\frac{C_e}{q_e} = \left(\frac{1}{K_L}\right)\left(\frac{1}{b}\right) + \left(\frac{1}{b}\right)C_e \tag{16}$$

where C_e is the equilibrium concentration (mg·L^{-1}), q_e is the amount of adsorbed species per gram of adsorbent (mg·g^{-1}), K_L is the Langmuir equilibrium constant, and b is the amount of adsorbate required to form a monolayer. Thus, a plot of C_e/q_e versus C_e should provide a straight line with a slope of $1/b$ and an intercept of $1/K_L b$, as shown in Figure 10. The values of K_L and b were calculated and are reported in Table 5.

A dimensionless equilibrium parameter or constant separation factor, R_L, was used to determine the applicability of the

Table 5. Related Isotherm Parameters for the Adsorption of Cu(II) and Ni(II) onto ADS at 293 K

	metal ions	
adsorption isotherms and its constants	Cu(II)	Ni(II)
Langmuir adsorption isotherm constants		
b ($mg \cdot g^{-1}$)	37.3	29.9
K_L ($L \cdot mg^{-1}$)	0.549	0.815
R^2	0.967	0.987
R_L	0.0894	0.0676
SSE	0.099	0.069
Freundlich adsorption isotherm constants		
K_F ($mg \cdot g^{-1}$) ($L \cdot mg^{-1}$)$^{1/n}$	2.957	2.540
N	5.959	6.211
R^2	0.979	0.979
SSE	0.444	0.339
Dubinin−Radushkevich isotherm constants		
$Y \cdot 10^8$ ($mol^2 \cdot J^{-2}$)	−0.331	−0.375
C_m ($mg \cdot g^{-1}$)	4.879	3.651
$E \cdot 10^4$ ($J \cdot mol^{-1}$)	1.229	1.553
R^2	0.930	0.932
SSE	0.743	0.590

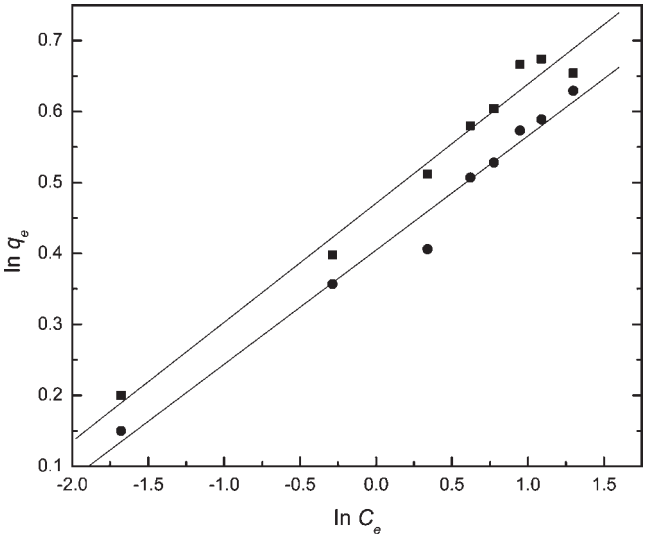

Figure 11. Freundlich isotherm plots of the adsorption on Cu(II) (■) and Ni(II) (●) onto ADS at 293 K.

Langmuir isotherms. The R_L of the adsorption of Cu(II) and Ni(II) ions was obtained from the following equation:[33,34]

$$R_L = \frac{1}{(1 + K_L[C_0])} \quad (17)$$

where K_L is the Langmuir constant ($L \cdot g^{-1}$) and $[C_0]$ is the highest initial metal ion concentration ($mg \cdot L^{-1}$). A R_L between 0 and 1 is indicative of a favorable adsorption process; however, a $R_L > 1$ represents an unfavorable process. Alternatively, if $R_L = 1$, adsorption is linear. Lastly, if $R_L = 0$, the adsorption process is irreversible.

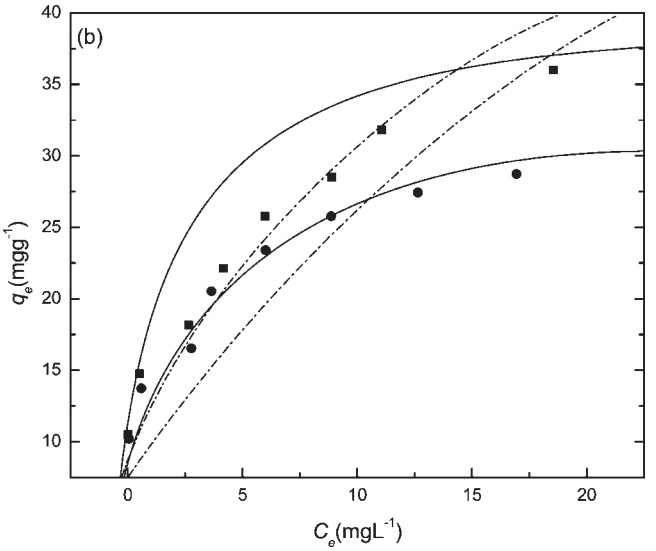

Figure 12. Validation of adsorption isotherms onto ADS (the solid line represents Langmuir and the broken line represents Freundlich isotherm) of Cu(II) (■) and Ni(II) (●) at 293 K.

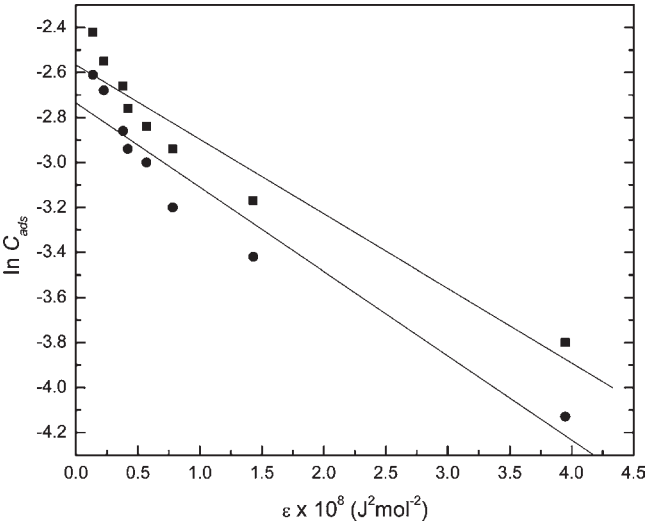

Figure 13. D-R isotherm plots of the adsorption on Cu(II) (■) and Ni(II) (●) onto ADS at 293 K.

As shown in Figure 10, the application of the Langmuir isotherm resulted in linearized data, and the correlation coefficient of the adsorption of Cu(II) and Ni(II) ions was 0.967 and 0.987, respectively. Moreover, the sum of the squares of error of Cu(II) and Ni(II) adsorption was 0.099 and 0.069, respectively, indicating that Cu(II) and Ni(II) ions adsorbed as a monolayer onto the surface of ADS. The Langmuir constant, b, which is a measure of the adsorption capacity of the monolayer, was 37.3 $mg \cdot g^{-1}$ for Cu(II) and 29.9 $mg \cdot g^{-1}$ for Ni(II) at 293 K. The dimensionless parameter, R_L, was 0.0894 and 0.0676 for Cu(II) and Ni(II) ions, respectively; thus, the R_L values are ($0 < R_L < 1$) consistent with a favorable adsorption process. Table 5 displays the calculated parameters of the Langmuir model.

Freundlich Isotherm Model. The Freundlich model[35] is applicable for nonideal sorption on heterogeneous surfaces and

Table 6. Comparison of Adsorption Capacities of Different Activated Carbon Adsorbents for Cu(II) and Ni(II) Removal

	q_m (mg·g^{-1})		adsorption condition		
activated carbons	Cu(II)	Ni(II)	temp. (K)	pH	refs
hazelnut husk carbon	6.64			5.7	13
rubber wood sawdust carbon	5.72			6	14
rice hulls carbon	3.92		293	5.3	15
hazelnut shell carbon	58.27		323	6	16
chestnut shell carbon	100		308	5	17
grapeseed carbon	48.78		308	5	17
palm shell carbon	18.6			3	19
palm shell carbon	30.8			5	19
apricot stones carbon	24.21	27.21		4.9(Cu), 6.2(Ni)	40
cassava peel carbon	52			6	41
P. aureus hulls carbon	19.5			6.9	42
hazelnut shell carbon		11.64	323		43
lotus stalks carbon		31.45	328		18
peanut hull carbon	65.6	53.65		5.0(Cu), 6.5(Ni)	45 and 46
commercial activated carbon	3.6	1.49		5.0(Cu), 6.5(Ni)	45 and 46
R. communis Pericarp carbon		31.15		5	47
coir pith carbon	39.7	62.5	303	4.2(Cu), 5.0(Ni)	48 and 49
P. dactylifera stone carbon	37.3	29.9	293	6.0(Cu), 5.5(Ni)	this study

multilayer adsorption processes. According to the Freundlich model:

$$q_e = K_F(C_e)^{1/n} \quad (18)$$

$$\ln q_e = \ln K_F + \frac{1}{n}\ln C_e \quad (19)$$

where K_F is Freundlich equilibrium constant and n is an empirical constant. Thus, a plot of ln q_e vs ln C_e should provide a straight line with a slope of $(1/n)$ and an intercept of ln(K_F), as shown in Figure 11. The correlation coefficients for the adsorption of Cu(II) and Ni(II) ions were 0.979 and 0.979, and the SSE values were 0.444 and 0.339, respectively. The parameters of the Freundlich model are reported in Table 5.

Figure 12 represents the adsorption isotherm of ADS along with its validation with the Langmuir and Freundlich isotherms.

Dubinin−Radushkevich (D-R) Isotherm Model. To determine whether the adsorption is physical or chemical in nature, the equilibrium data were applied to the D-R model.[36] The linearized form of the D-R model is provided below:

$$\ln C_{ads} = \ln C_m - Y\varepsilon^2 \quad (20)$$

where C_{ads} is the concentration of adsorbed metal ions on the surface of the adsorbent (mg·L^{-1}), C_m is the maximum adsorption capacity (mg·g^{-1}), Y is the activity coefficient related to the mean adsorption energy (mol^2·J^{-2}), and ε is the Polanyi potential (kJ^2·mol^2). The Polanyi potential[37] can be calculated from the following equation:

$$\varepsilon = RT\ln\left(1 + \frac{1}{C_e}\right) \quad (21)$$

The mean adsorption energy, E (kJ·mol^{-1}), is calculated from the following equation:

$$E = \frac{1}{\sqrt{-2Y}} \quad (22)$$

As shown in Figure 13, the plot of ln C_{ads} versus ε^2 (eq 20) is a straight line, and the values of Y and C_m for Cu(II) and Ni(II) ions were obtained. The adsorption potential is independent of the temperature; however, the nature of the adsorbent and the adsorbate has an effect on the adsorption potential. The mean free energy of adsorption, E, which is the free energy associated with the transfer of one mole of metal ions from the solution to the surface of the adsorbent, indicates whether the adsorption process occurs via ion exchange or physical adsorption. If the value of E lies between 8 and 16 kJ·mol^{-1}, the adsorption process occurs due to ion-exchange; however, if E < 8 kJ·mol^{-1}, the adsorption process is based on physical interactions.[38,39] The mean adsorption energy of Cu(II) and Ni(II) ion adsorption was 12.29 kJ·mol^{-1} and 15.53 kJ·mol^{-1} (Table 5), respectively, which suggests that chemisorption was the dominant process. Alternatively, the observed values of E may suggest that adsorption is accompanied by ion exchange at the surface of the adsorbent.

Compared to the Freundlich and D-R adsorption isotherm models, the Langmuir adsorption isotherm model provided the highest R^2 values and lowest SSE values for both metal ions; thus, the Langmuir model best fits the experimental data.

Table 6 presents a clear picture of the comparison of adsorption capacities for the removal of Cu(II) and Ni(II) by different biomass-based activated carbons. On perusal of this table, it can be inferred that ADS have comparable adsorption capacity to that of hazelnut and chestnut shell based activated carbons in case of Cu(II) removal and lotus stalk and *Ricinus communis* Pericarp based activated carbon in case of Ni(II) adsorption.

CONCLUSIONS

In this study, characterization of activated carbon obtained from *Phoenix dactylifera* stone has been done. Further, batch adsorption experiments for the removal of Cu(II) and Ni(II) ions from aqueous solutions were conducted with ADS, which is

a readily available agricultural byproduct in Middle-Eastern countries. The percent adsorption of Cu(II) and Ni(II) ions increased with an increase in contact time and initial metal ion concentration. The rate of adsorption conformed to pseudosecond-order kinetics, and an excellent correlation was obtained for this model. Equilibrium data fit the Langmuir adsorption isotherm model, confirming monolayer adsorption on the surface of ADS for Cu(II) and Ni(II) ions at 293 K. The thermodynamic calculations suggested that the adsorption process is spontaneous and exothermic in nature. Based on the above results, it can be concluded that ADS is a suitable adsorbent for the removal of Cu(II) and Ni(II) ions from aqueous solution. Moreover, ADS is a natural, low cost, and abundant material. Further studies on the adsorption of other metals and the corresponding kinetics in a fixed bed of date stone under continuous and recirculating modes should provide pertinent rate data necessary for the design of large scale, continuous adsorption processes. In addition, to optimize the treatment of industrial wastewaters that contain a variety of different metal ions, the mechanism of adsorption by activated date stone and the effect of coadsorption of multiple metals on the sorption capacity should be investigated.

■ ASSOCIATED CONTENT

Supporting Information. Additional Lagergren, Elovich, and Weber−Morris plots. This material is available free of charge via the Internet at http://pubs.acs.org.

■ AUTHOR INFORMATION

Corresponding Author

*Tel.: +604-653-5217/2260/5219. Fax: +604-657-3678. E-mail: mdanishchem@gmail.com.

Funding Sources

The authors acknowledge the Research University Postgraduate Research Grant Scheme (1001/PTEKIND/844042) for funding the research and Universiti Sains Malaysia for the Fellowship provided to M.D.

■ REFERENCES

(1) Panday, K. K.; Gur, P.; Singh, V. N. Copper (II) removal from aqueous solutions by fly ash. *Water Res.* **1985**, *19*, 869–873.

(2) Camp, R. T. *Water and its impurities*, 2nd ed.; Reinhold: New York, 1964.

(3) Rao, C. S. *Environmental pollution control Engineering*; Wiley Eastern Limited: New Delhi, 1992.

(4) Rao, P. S.; Reddy, K. V. N. S.; Kalyani, S.; Krishnaiah, A. Comparative sorption of copper and nickel from aqueous solutions by natural neem (*Azadirachta indica*) sawdust and acid treated sawdust. *Wood Sci. Technol.* **2007**, *41*, 427–442.

(5) WHO *Guidelines for Drinking Water Quality*, 2nd ed.; World Health Organization: Geneva

(6) Ho, Y. S.; Huang, C. T.; Huang, H. W. Equilibrium sorption isotherm for metal ions on tree fern. *Process Biochem.* **2002**, *37*, 1421–1430.

(7) Suzuki, M. Role of adsorption in water environment processes. *Water Sci. Technol.* **1997**, *35*, 01–11.

(8) Chandra, S. K.; Subramanian, S.; Modak, J. M.; Natarajan, K. A. Removal of metal ions using an industrial biomass with references to environmental control. *Int. J. Miner. Process* **1998**, *53*, 107–120.

(9) Bansode, R. R.; Losso, J. N.; Marshall, W. E.; Rao, R. M.; Portier, R. J. Adsorption of metal ions by pecan shell-based granular activated carbons. *Bioresour. Technol.* **2003**, *89*, 115–119.

(10) Huang, C. P.; Corapcioglu, M. O. The adsorption of heavy metals on to hydrous activated carbon. *Water Res.* **1987**, *21*, 1031–1044.

(11) Ali, I.; Gupta, V. K. Advances in water treatment by adsorption technology. *Nat. Protoc.* **2006**, *1*, 2661–2667.

(12) Gupta, V. K.; Carrott, P. J. M.; Ribeiro Carrott, M. M. L.; Suhas Low-cost adsorbents: Growing approach to wastewater treatment-a review. *Crit. Rev. Env. Sci. Tec.* **2009**, *39*, 783–842.

(13) Imamoglu, M.; Tekir, O. Removal of copper (II) and lead (II) ions from aqueous solutions by adsorption on activated carbon from a new precursor hazelnut husks. *Desalination* **2008**, *228*, 108–113.

(14) Kalavathy, M. H.; Karthikeyan, T.; Rajgopal, S.; Miranda, L. R. Kinetic and isotherm studies of Cu(II) adsorption onto H_3PO_4-activated rubberwood sawdust. *J. Colloids Interf. Sci.* **2005**, *292*, 354–362.

(15) Teker, M.; Imamoglu, M.; Saltabas, O. Adsorption of copper and cadmium ions by activated carbon from rice hulls. *Turk. J. Chem.* **1999**, *23*, 185–191.

(16) Demirbas, E.; Dizge, N.; Sulak, M. T.; Kobya, M. Adsorption kinetics and equilibrium of copper from aqueous solutions using hazelnut shell activated carbon. *Chem. Eng. J.* **2009**, *148*, 480–487.

(17) Ozçimen, D.; Ersoy-Meriçboyu, A. Removal of copper from aqueous solutions by adsorption onto chestnut shell and grapeseed activated carbons. *J. Hazard. Mater.* **2009**, *168*, 1118–1125.

(18) Huang, L. H.; Sun, Y. Y.; Yang, T.; Li, L. Adsorption behavior of Ni (II) on lotus stalks derived active carbon by phosphoric acid activation. *Desalination* **2011**, *268*, 12–19.

(19) Issabayeva, G.; Aroua, M. K.; Sulaiman, N. M. Study on palm shell activated carbon adsorption capacity to remove copper ions from aqueous solutions. *Desalination* **2010**, *262*, 94–98.

(20) Danish, M.; Hashim, R.; Rafatullah, M.; Sulaiman, O.; Ahmad, A.; Govind Adsorption of Pb(II) ions from aqueous solutions by date bead carbon activated with $ZnCl_2$. *Clean-Soil, Air, Water* **2011**, *39*, 392–399.

(21) Reed, A. R.; Williums, P. T. Thermal processing of biomass natural fiber wastes by pyrolysis. *Int. J. Energy Res.* **2004**, *28*, 131–145.

(22) Panda, G. C.; Das, S. K.; Bandopadhyay, T. S.; Guha, A. K. Adsorption of nickel on husk of lathyrus sativus: Behavior and binding mechanism. *Colloids Surf., B* **2007**, *57*, 135–142.

(23) Danish, M.; Sulaiman, O.; Rafatullah, M.; Hashim, R.; Ahmad, A. Kinetics for the removal of Paraquat Dichloride from aqueous solution by activated date (*Phoenix dactylifera*) stone carbon. *J. Dispersion Sci. Technol.* **2010**, *31*, 248–259.

(24) Lagergren, S. About the theory of so called adsorption of soluble substances, kungliga Svenska Vetenskapsakademiens. *Handlingar* **1898**, *24*, 1–39.

(25) Ho, Y. S.; McKay, G. A comparison of chemisorptions kinetic models applied to pollutant removal on various sorbents. *Trans. IChE* **1998**, *76B*, 332–340.

(26) Juang, R.; Chen, M. Application of the Elovich equation to the kinetics of metal sorption with solvent-impregnated resins. *Ind. Eng. Chem. Res.* **1997**, *36*, 813–820.

(27) Weber, W. J.; Morris, J. C. Kinetics of adsorption on carbon from solution. *J. Sanit. Eng. Div. Am. Soc. Civ. Eng.* **1963**, *89*, 31–60.

(28) McKay, G.; Al-Duri, B. Study of the mechanism of pore diffusion in batch adsorption systems. *J. Chem. Technol. Biotechnol.* **1990**, *48*, 269–275.

(29) Ghaedi, M.; Shokrollahi, A.; Hossainian, H.; Kokhdan, S. N. Comparison of activated carbon and multiwalled carbon nanotubes for efficient removal of eriochrome cyanine R(ECR): Kinetic, isotherm, and thermodynamic study of the removal process. *J. Chem. Eng. Data* dx.doi.org/10.1021/je200331u

(30) Dogan, M.; Alkan, M. Adsorption kinetics of methyl violet onto perlite. *Chemosphere* **2003**, *50*, 517–528.

(31) Ho, Y. S.; Ng, J. C. Y.; McKay, G. Kinetics of pollution sorption by biosorbents-Review. *Sep. Purif. Methods* **2000**, *29*, 189–232.

(32) Langmuir, I. The adsorption of gases on plane surfaces of glass, mica and platinum. *J. Am. Chem. Soc.* **1918**, *40*, 1361–1403.

(33) Hall, K. R.; Eagleton, L. C.; Acrivos, A.; Vermeulen, T. Pore and solid diffusion kinetics in fixed bed adsorption under constant pattern conditions. *Ind. Eng. Chem. Fundam.* **1966**, *5*, 212–219.

(34) Weber, T. W.; Chakraborti, R. K. Pore and solid diffusion models for fixed bed adsorbents. *J. Am. Inst. Chem. Eng.* **1974**, *20*, 228–238.

(35) Freundlich, H. Ueber die adsorption in Loesungen. *Z. Phys. Chem.* **1907**, *57*, 385–470.

(36) Dubinin, M. M.; Zaverina, E. D.; Radushkevich, L. V. Sorption and structure of activated carbons. I. Adsorption of organic vapours. *Zh. Fiz. Khim.* **1947**, *21*, 1351–1362.

(37) Polanyi, M. Theories of the adsorption of gases. A general survey and some additional remarks. *Trans. Faraday Soc.* **1932**, *28*, 316–332.

(38) Helfferich, F. *Ion Exchange*; McGraw-Hill: New York, 1962.

(39) Saltali, K.; Sari, A.; Aydin, M. Removal of ammonium ions from aqueous solution by natural Turkish (Yildizeli) zeolite for environmental quality. *J. Hazard. Mater.* **2006**, *B141*, 258–263.

(40) Kobya, M.; Demirbas, E.; Senturk, E.; Ince, M. Adsorption of heavy metal ions from aqueous solutions by activated carbon prepared from apricot stone. *Bioresour. Technol.* **2005**, *96*, 1518–1521.

(41) Moreno-Piraján, J. C.; Giraldo, L. Adsorption of copper from aqueous solution by activated carbons obtained by pyrolysis of cassava peel. *J. Anal. Appl. Pyrolysis* **2010**, *87*, 188–193.

(42) Rao, M. M.; Ramana, D. K.; Seshaiah, K.; Wang, M. C.; Chien, S. W. C. Removal of some metal ions by activated carbon prepared from Phaseolus aureus hulls. *J. Hazard. Mater.* **2009**, *166*, 1006–1013.

(43) Demirbas, E.; Kobya, M.; Öncel, S.; Sencan, S. Removal of Ni(II) from aqueous solution by adsorption onto hazelnut shell activated carbon: equilibrium studies. *Bioresour. Technol.* **2002**, *84*, 291–293.

(44) Huang, L.; Sun, Y.; Yang, T.; Li, L. Adsorption behavior of Ni (II) on lotus stalks derived active carbon by phosphoric acid activation. *Desalination* **2011**, *268*, 12–19.

(45) Periasamy, K.; Namasivayam, C. Removal of Nickel(II) from aqueous solution and nickel plating industry wastewater using an agricultural waste: Peanut hulls. *Waste Manage.* **1995**, *15*, 63–68.

(46) Periasamy, K.; Namasivayam, C. Removal of Copper (II) by adsorption onto Peanut hull carbon from water and copper plating industry wastewater. *Chemosphere* **1996**, *32*, 769–789.

(47) Madhavakrishnan, S.; Manickavasagam, K.; Rasappan, K.; Shabudeen, P. S. S.; Venkatesh, R.; Pattabhi, S. *Ricinus Communis* pericarp activated carbon used as an adsorbent for the removal of Ni(II) from aqueous solution. *E-J. Chem.* **2008**, *5*, 761–769.

(48) Kadirvelu, K.; Thamaraiselvi, K.; Namasivayam, C. Adsorption of nickel (II) from aqueous solution onto activated carbon prepared from coirpith. *Sep. Purif. Technol.* **2001**, *24*, 497–505.

(49) Namasivayam, C.; Kadirvelu, K. Agricultural solid wastes for the removal of heavy metals: Adsorption of Cu(II) by coirpith carbon. *Chemosphere* **1997**, *34*, 377–399.